Measurements of the L-shell x-ray production cross sections of Yb and Au by Li, Be, C, N, F, and Si bombardments

N. B. Malhi and T. J. Gray
J. R. Macdonald Laboratory, Department of Physics, Kansas State University, Manhattan, Kansas 66502
(Received 5 August 1991)

L-shell x-ray production cross sections for $L\alpha_{1,2}$, $L\gamma_1$, and $L\gamma_{2,3,(6)}$ have been measured for ^{7}Li, ^{9}Be, ^{12}C, ^{14}N, ^{19}F, and ^{28}Si on Yb and Au. The energy ranges for the incident ion species were 0.5–3.0 MeV/μ for Li, Be, C, and F, and 0.5–2.6 MeV/μ for N and Si. Comparisons of the $L\alpha_{1,2}$ and $L\gamma_{2,3,(6)}$ x-ray production-cross-section data have been made to the prediction of plane-wave Born-approximation theory and perturbed-stationary-state theory with energy-loss, Coulomb deflection, and relativistic corrections (ECPSSR). The comparison shows that for the $L\gamma_{2,3,(6)}$ x-ray production cross sections there are problems associated with the ECPSSR theory.

PACS number(s): 34.50.Fa

I. INTRODUCTION

A large variety of measurements of L x-ray production cross sections by incident ions have been carried out during the past two decades, most of the measurements having concentrated on low projectile atomic number.

In an attempt to understand the energy dependence of $L_{\rm I}$-, $L_{\rm II}$-, and $L_{\rm III}$-subshell ionization cross sections, earlier measurements [1–5] of L-subshell ionization and x-ray production have been compared to the predictions of first-order direct Coulomb ionization theories, such as plane-wave Born approximation (PWBA) [6] and perturbed-stationary-state theory with energy-loss, Coulomb deflection, and relativistic corrections (ECPSSR) [7]. This comparison has shown a discrepancy between experiment and theories, which were more pronounced for high-projectile atomic number. More sensitive tests of these theories have been done [8] when we compared the experimental ratios of the x-ray intensities of $L\alpha_{1,2}$ to $L\gamma_{2,3,(6)}$ for light and heavy projectiles with the same theoretical ratios calculated via PWBA and ECPSSR theories. Both theories failed to explain the behavior in the ratios as projectile atomic number (Z_1) and energy (E/M) were varied. Recently, the experimental x-ray production cross sections $\sigma_{L\gamma_{2,3,(6)}}$ for H, Li, N, and Si on Yb have been compared to the calculations of these cross sections via an approach based upon coupled-channel calculations [9]. Improved agreement between the data and theory for the $L\gamma_{2,3,(6)}$ x-ray production cross sections was obtained using the coupled-channel approach.

The present paper presents the experimental x-ray production cross sections $\sigma_{L\alpha_{1,2}}$, $\sigma_{L\gamma_1}$, and $\sigma_{L\gamma_{2,3,(6)}}$ for Li, Be, C, N, F, and Si on Yb ($Z_2=70$) and Au ($Z_2=79$) targets.

II. EXPERIMENTAL PROCEDURE AND DATA ANALYSIS

Beams of Li, Be, C, N, F, and Si ions were accelerated by a 7-MV tandem Van de Graaff accelerator at Kansas State University (J. R. Macdonald Laboratory). Thin targets were prepared by vacuum evaporation of Yb onto 20-μg/cm^2 carbon foil backings, and self-supporting Au foils were also made. The accelerated beams were directed toward the target foil which is mounted at 45° with respect to the incident beam direction. The x rays were detected with an Ortec Si(Li) detector, which was coupled to the vacuum system of the scattering chamber at an angle of 90° to the incident beam direction. The energy resolution was measured to be $\Delta E_{\rm FWHM}\simeq 168$ eV (where FWHM denotes full width at half maximum) at 5.895 keV. A thin polyester tape mounted in front of the

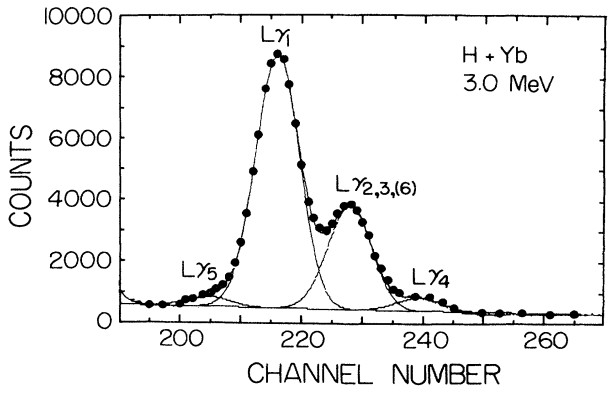

FIG. 1. A typical $L\gamma$ x-ray spectra and the results of a computer fit to the x-ray energy spectrum.

TABLE I. X-ray production cross sections $\sigma_{L\alpha_{1,2}}$ of Yb for ^{7}Li, ^{9}Be, ^{12}C, ^{14}N, ^{19}F, and ^{28}Si ions. Relative errors are 10%.

E_p (MeV/μ)	Li (barns)	Be (barns)	C (barns)	N (barns)	F (barns)	Si (barns)
3.0	668	1221	1962		7184	
2.9	651	1142	1750		6199	
2.8	659	1035	1648	2800	5587	17 650
2.7	566	1072	1556		5340	15 460
2.6	513	949	1448	2702	4762	14 340
2.5	487	880	1326	2493	4404	12 960
2.4	454	800	1204	2323	3894	11 320
2.3	440	729	1068	2104	3449	9 603
2.2	422	620	939	1709	3083	9 731
2.1	364	623	780	1585	2728	8 664
2.0	324	514	672	1360	2494	6 974
1.9	280	447	600	1199	2011	6 565
1.8	254	393	521	1032	1895	5 396
1.7	226	371	451	898	1526	4 655
1.6	184	284	399	713	1298	3 662
1.5	165	260	341	596	1088	3 155
1.4	135	208	288	506	919	2 575
1.3	120	180	248	467	754	1 735
1.2	98.8	155	205	358	544	1 489
1.1	82.0	121	168	249	408	861
1.0	62.6	104	140	191	311	670
0.9	50.0	71.9	113	146	238	440
0.8	39.5	51.5	79.3	93.0	202	325
0.7	25.6	31.8	50.0	65.0	129	178
0.6	16.1	20.5	35.6	26.0	97.6	94.8
0.5	9.3		16.5	14.0	29.8	56.6

TABLE II. X-ray production cross sections $\sigma_{L\gamma_1}$ of Yb for ^{7}Li, ^{9}Be, ^{12}C, ^{14}N, ^{19}F, and ^{28}Si ions. Relative errors are 15% for Li, Be, C, and N; 20% for F; and 25% for Si ions.

E_p (MeV/μ)	Li (barns)	Be (barns)	C (barns)	N (barns)	F (barns)	Si (barns)
3.0	51.5	95	142		432	
2.9	49.5	85	126		368	
2.8	48.5	78	117	196	330	908
2.7	42.6	80	110		309	767
2.6	38.7	71	102	187	279	704
2.5	36.6	66.0	92.0	165	251	602
2.4	34.0	60.1	82.7	155	220	507
2.3	32.6	53.9	72.7	138	192	418
2.2	31.0	45.2	64.4	113	171	411
2.1	26.6	44.8	53.9	103	149	355
2.0	23.8	39.9	46.4	88.6	135	272
1.9	20.4	32.0	40.4	78.2	109	246
1.8	18.4	28.0	34.9	67.8	103	200
1.7	16.1	25.9	29.9	57.7	82.6	166
1.6	13.0	20.1	26.8	46.3	71.0	127
1.5	11.5	18.0	23.0	39.0	59.3	108
1.4	9.4	15.0	19.4	33.2	50.8	91.1
1.3	8.3	12.2	16.9	30.6	42.4	60.8
1.2	6.9	10.9	14.0	23.8	31.4	55.5
1.1	5.5	8.5	11.7	16.8	24.4	33.2
1.0	4.3	7.5	9.8	13.1	19.2	26.4
0.9	3.5	5.2	8.1	10.4	15.1	17.7
0.8	2.8	3.7	5.8	6.8	13.0	12.9
0.7	1.8	2.4	3.8	4.9	8.5	7.1
0.6	1.2	1.6	2.9	2.1	6.6	3.8
0.5	0.7		1.4	1.3	2.2	2.4

detector was used to attenuate the strong M-shell x rays. Simultaneous with x-ray detection, the scattered ions were detected by a surface barrier detector mounted in vacuum at a laboratory angle of 135° with respect to the incident beam direction.

Consistent fitting procedures were important mainly because the $L\gamma$ lines were not fully resolved for high-Z projectiles due to the inherent x-ray detector resolution limitations and spectral broadening associated with multiple M- and N-shell ionization. The peak intensities were extracted using a fitting program developed by Stökli [10], which is capable of fitting multiple Gaussian and non-Gaussian peaks on a linear or higher-order background. A typical $L\gamma$ x-ray spectrum and the results of a computer fit to the x-ray energy spectrum for H on Yb is shown in Fig. 1.

The experimental x-ray production cross sections σ_{x_i} were obtained from the data as follows:

$$\sigma_{x_i} = C \left[\frac{Y_{x_i}}{Y_p} \right] \left[\frac{Z_1}{E_p} \right]^2 ,$$

where Y_{x_i} is the measured x-ray yield, Y_p is the yield or the number of elastically scattered ions, Z_1 and E_p are the projectile atomic number and energy (MeV), respectively. The constant of proportionality C was determined

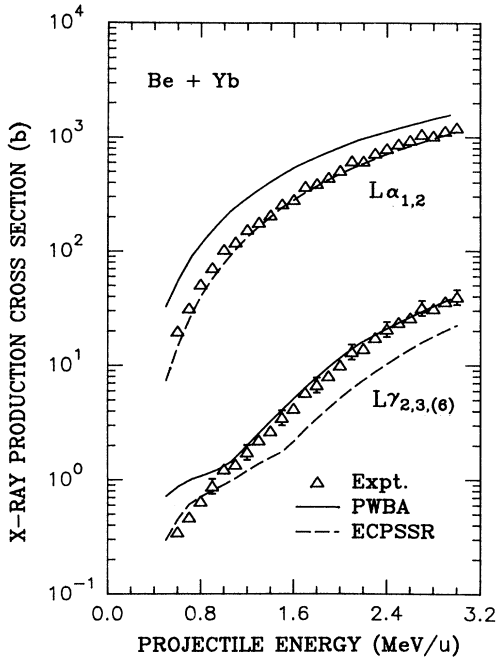

FIG. 2. X-ray production cross sections $\sigma_{L\alpha_{1,2}}$ and $\sigma_{L\gamma_{2,3,(6)}}$ for Be on Yb compared to PWB and ECPSSR theories.

TABLE III. X-ray production cross sections $\sigma_{L\gamma_{2,3,(6)}}$ of Yb for ^{7}Li, ^{9}Be, ^{12}C, ^{14}N, ^{19}F, and ^{28}Si ions. Relative errors are 15% for Li, Be, C, and N; 20% for F; and 25% for Si ions.

E_p (MeV/μ)	Li (barns)	Be (barns)	C (barns)	N (barns)	F (barns)	Si (barns)
3.0	21.3	39.9	66.6		241	
2.9	20.3	36.4	57.6		201	
2.8	19.6	31.6	52.7	83.0	173	475
2.7	16.1	32.0	48.3		159	405
2.6	13.8	26.3	42.0	78.6	137	344
2.5	12.6	23.9	37.7	70.6	123	307
2.4	11.2	20.9	31.9	62.6	103	254
2.3	10.3	17.6	27.5	54.6	87.7	203
2.2	9.2	14.1	22.5	42.5	74.2	192
2.1	7.4	13.2	17.9	37.3	64.2	171
2.0	6.2	10.1	14.6	30.5	56.5	134
1.9	4.9	8.1	12.5	26.0	44.8	121
1.8	4.2	6.8	10.1	20.9	41.8	96.6
1.7	3.4	5.8	8.5	17.6	31.9	84.2
1.6	2.5	4.2	7.1	13.9	26.9	65.0
1.5	2.0	3.5	5.7	11.1	22.3	59.5
1.4	1.5	2.7	4.7	9.1	18.7	49.5
1.3	1.3	2.2	3.9	8.0	15.2	36.8
1.2	0.95	1.8	3.1	6.0	11.4	34.8
1.1	0.78	1.4	2.6	4.2	8.6	22.0
1.0	0.60	1.2	2.1	3.2	6.6	17.9
0.9	0.50	0.88	2.5	2.5	5.3	12.1
0.8	0.46	0.65	1.2	1.5	4.5	8.8
0.7	0.37	0.47	0.77	1.1	2.9	4.8
0.6	0.29	0.35	0.58	0.68	2.2	2.6
0.5	0.23		0.30	0.40	0.66	1.7

TABLE IV. X-ray production cross sections $\sigma_{L\alpha_{1,2}}$, $\sigma_{L\gamma_1}$, and $\sigma_{L\gamma_{2,3,(6)}}$ of Au for ^{7}Li and ^{9}Be ions. Relative errors are 10% in $\sigma_{L\alpha_{1,2}}$, and 15% in $\sigma_{L\gamma_1}$ and $\sigma_{L\gamma_{2,3,(6)}}$.

E_p (MeV/μ)	$\sigma_{L\alpha_{1,2}}$ (barns)	$\sigma_{L\gamma_1}$ (barns)	$\sigma_{L\gamma_{2,3,(6)}}$ (barns)	E_p (MeV/μ)	$\sigma_{L\alpha_{1,2}}$ (barns)	$\sigma_{L\gamma_1}$ (barns)	$\sigma_{L\gamma_{2,3,(6)}}$ (barns)
3.0	330	23.0	7.0	3.0	499	33.6	10.2
2.9	315	21.9	6.7	2.9	477	31.2	9.4
2.8	316	22.1	6.4	2.8	441	29.2	8.6
2.7	291	20.2	5.6	2.7	439	29.3	8.5
2.6	240	16.5	4.5	2.6	380	25.6	7.2
2.5	215	14.8	3.9	2.5	375	25.0	6.8
2.4	190	13.0	3.3	2.4	301	20.1	5.3
2.3	177	12.2	3.0	2.3	285	19.0	4.8
2.2	171	11.6	2.7	2.2	247	16.4	4.0
2.1	140	9.5	2.2	2.1	240	15.9	3.8
2.0	115	7.8	1.8	2.0	204	13.5	3.1
1.9	106	7.1	1.6	1.9	173	11.4	2.6
1.8	95.2	6.4	1.4	1.8	156	10.2	2.2
1.7	83.6	5.6	1.2	1.7	132	8.7	1.9
1.6	76.2	5.1	1.1	1.6	111	7.4	1.6
1.5	68.3	4.5	0.95	1.5	101	6.6	1.5
1.4	57.2	3.8	0.80	1.4	83.9	5.5	1.2
1.3	45.4	3.0	0.66	1.3	72.7	4.8	1.1
1.2	36.0	2.4	0.54	1.2	51.6	3.4	0.79
1.1	32.0	2.1	0.49	1.1	46.7	3.8	0.79
1.0	24.3	1.6	0.41	1.0	34.7	2.4	0.61
0.9	17.5	1.2	0.32	0.9	26.7	1.9	0.53
0.8	12.3	0.80	0.25	0.8	23.7	1.7	0.51
0.7	9.1	0.60	0.22	0.7	15.1	1.1	0.37
0.6				0.6	3.9	0.31	0.11

TABLE V. X-ray production cross sections $\sigma_{L\alpha_{1,2}}$, $\sigma_{L\gamma_1}$, and $\sigma_{L\gamma_{2,3,(6)}}$ of Au for ^{12}C and ^{14}N ions. Relative errors are 10% in $\sigma_{L\alpha_{1,2}}$, and 15% in $\sigma_{L\gamma_1}$ and $\sigma_{L\gamma_{2,3,(6)}}$.

E_p (MeV/μ)	$\sigma_{L\alpha_{1,2}}$ (barns)	$\sigma_{L\gamma_1}$ (barns)	$\sigma_{L\gamma_{2,3,(6)}}$ (barns)	E_p (MeV/μ)	$\sigma_{L\alpha_{1,2}}$ (barns)	$\sigma_{L\gamma_1}$ (barns)	$\sigma_{L\gamma_{2,3,(6)}}$ (barns)
3.0	1032	67.1	23.8				
2.9	969	63.3	21.7				
2.8	904	58.5	19.8	2.79	775	48.8	16.2
2.7	819	52.8	17.2				
2.6	690	44.6	14.0	2.59	712	44.1	14.4
2.5	584	38.2	11.9	2.49	707	45.9	14.2
2.4	553	36.0	10.7	2.39	660	41.6	12.8
2.3	465	30.2	8.8	2.29	595	37.8	11.6
2.2	440	28.7	8.2	1.19	516	33.2	10.0
2.1	351	23.2	6.4	2.09	442	28.3	8.3
2.0	329	21.8	6.0	1.99	416	27.0	7.8
1.9	266	18.5	5.2	1.89	361	23.7	6.7
1.79	241	16.5	4.6	1.79	304	20.1	5.5
1.69	203	14.2	3.8	1.69	257	17.4	4.7
1.49	156	11.2	3.0	1.49	179	12.3	3.3
1.39	143	10.1	2.6	1.38	147	10.3	2.8
1.29	119	9.0	2.5	1.29	129	9.0	2.4
1.19	91.7	7.0	2.0	1.19	101	7.4	2.0
1.09	76.5	5.7	1.6	1.09	80.6	6.1	1.6
0.99	67.0	5.4	1.5	0.98	65.3	5.0	1.3
0.89	47.8	4.0	1.2	0.88	47.0	3.8	1.1
0.79	30.7	2.5	0.72	0.78	41.7	3.4	0.94
0.69				0.68	27.4	2.5	0.71
0.58	11.6	1.1	0.34	0.57	14.7	1.5	0.41

by normalizing to known measurements of σ_{x_i}. Our measured x-ray production cross sections for the Yb target were normalized to a measured $L\alpha_{1,2}$ x-ray production cross section $\sigma_{L\alpha_{1,2}}$, for 3.0-MeV/μ Li on Yb reported by Gray *et al.* [4]. For the Au target the normalization constant was determined using the measured cross section $\sigma_{L\alpha_{1,2}}$ for 3.0-MeV/μ H on Au [1]. The yields Y_{x_i} and Y_p were corrected for dead time which was recorded for each projectile energy for both the Yb and Au targets.

III. RESULTS AND DISCUSSIONS

The x-ray production cross sections $\sigma_{L\alpha_{1,2}}$ for Li, Be, C, N, F, and Si ions on Yb are listed in Table I; the errors in these cross sections are 10–15 %, with the larger errors for higher-projectile atomic number. Table II lists the measured x-ray production cross sections $\sigma_{L\gamma_1}$ for Li, Be, C, N, F, and Si on Yb. The errors in these measured cross sections range from 10% to 20%; they are 15% for F ions while they are 20% for Si ions. The measured x-ray production cross section $\sigma_{L\gamma_{2,3,(6)}}$ are listed in Table III for the same projectile ions, with higher errors which are 15% for Li, Be, C, and N; 20% for F; and 25% for Si ions.

Figure 2 shows the measured x-ray production cross sections $\sigma_{L\alpha_{1,2}}$ and $\sigma_{L\gamma_{2,3,(6)}}$ for Be on Yb compared to the predictions of the PWBA and ECPSSR theories. As the figure shows, in the case of $\sigma_{L\alpha_{1,2}}$ the PWBA overestimates the experimental cross sections, whereas the ECPSSR theory shows better agreement with the measured cross section. The comparison with the measured $L\gamma_{2,3,(6)}$ x-ray production cross sections shows that the PWBA is in good agreement with experiment at projectile energy $E_p \geq 1.0$ MeV/μ. On the other hand, it fails at lower projectile energies. The ECPSSR shows good agreement with experiment below 1.0-MeV/μ projectile energy, but it underestimates the experimental cross sections at higher projectile energies.

Figure 3 shows a comparison between PWBA and ECPSSR theories and the experimental cross sections $\sigma_{L\alpha_{1,2}}$ and $\sigma_{L\gamma_{2,3,(6)}}$ for N on Yb. As the figure indicates, we see that the same discrepancy between theory and experiment is persistent for the PWBA calculations of $\sigma_{L\alpha_{1,2}}$, while the ECPSSR theory shows good agreement with the data. The general trends of experimental cross sections $\sigma_{L\gamma_{2,3,(6)}}$, in Fig. 3, when compared to PWBA shows the same behavior as for Be on Yb. A larger discrepancy is noticed at the lower projectile energies; at the same time the underestimation of the experimental cross sections $\sigma_{L\gamma_{2,3,(6)}}$ increases when compared to ECPSSR theory. Similar behavior is seen in Fig. 4 when comparing $\sigma_{L\alpha_{1,2}}$ and $\sigma_{L\gamma_{2,3,(6)}}$ with the predictions of PWBA and ECPSSR theories for F ions incident upon Yb. The ionization cross sections calculated via PWBA and ECPSSR theories have been converted into x-ray production cross sections by using the single-hole radiative [11] and nonradiative [12] parameters.

Since the cross sections σ_{x_i} are measured at a particular energy, then it would be necessary to know the projectile energy E_p used to determine σ_{x_i}. Due to the thick-

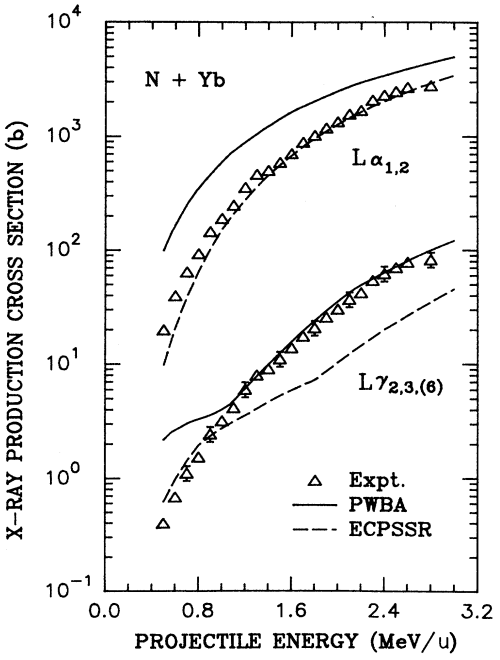

FIG. 3. X-ray production cross sections $\sigma_{L\alpha_{1,2}}$ and $\sigma_{L\gamma_{2,3,(6)}}$ for N on Yb compared to PWBA and ECPSSR theories.

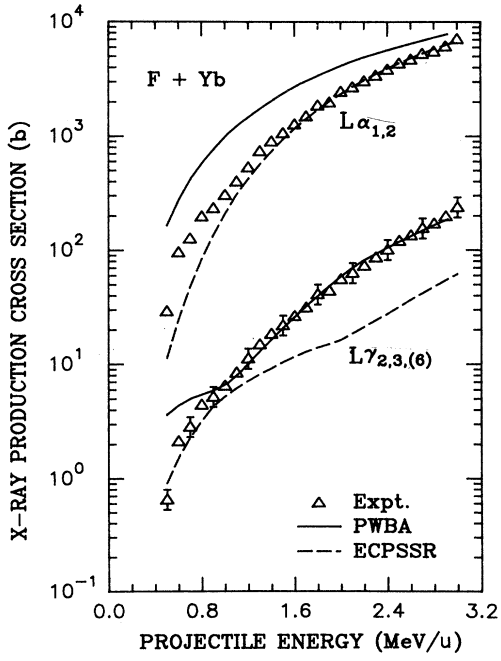

FIG. 4. X-ray production cross sections $\sigma_{L\alpha_{1,2}}$ and $\sigma_{L\gamma_{2,3,(6)}}$ for F on Yb compared to PWBA and ECPSSR theories.

ness of the target foil, the energy loss was determined for the Au target foil; the Yb foil was thin enough so the energy loss was much less than 1%, but this was not the case for the thicker Au foil. So the data presented in the forthcoming tables are presented with corrected projectile energies. The format for Tables IV–VI are different from Tables I–III because of the energy-loss corrections applied to the incident projectile energies in the case of the Au target. Table IV lists the measured x-ray production cross sections $\sigma_{L\alpha_{1,2}}$, $\sigma_{L\gamma_1}$, and $\sigma_{L\gamma_{2,3,(6)}}$ for Li and Be on Au target foil; the errors are the same as for Li and Be on Yb. The x-ray production cross sections $\sigma_{L\alpha_{1,2}}$, $\sigma_{L\gamma_1}$, and $\sigma_{L\gamma_{2,3,(6)}}$ for C and N on Au are listed in Table V, while Table VI presents the same cross sections for F and Si on the Au target.

The disagreement between the experimental data for the $L\gamma_{2,3,(6)}$ x-ray production cross section and theories employed in the comparison indicates that there is a problem in the target electron momentum distribution for the $2s$ state, where the theories use a hydrogenic wave function as an initial state in their formalism. The ECPSSR calculations include entrance channel interactions between the projectile and bound electron through consideration of binding energy and polarization effects in the framework of a perturbed-stationary-state approach. While this type of calculation does improve agreement between theory and experiment in the case of the $L_{\alpha_{1,2}}$ x-ray production cross sections, it is shown in this work that the ECPSSR calculations do not agree with the experimental data for the $L_{\gamma_{2,3,(6)}}$ x-ray production cross sections. The structure in the energy dependence of the $L_{\gamma_{2,3,(6)}}$ cross section associated with the $2s$ character of the bound electron clearly washes out in the experimental data as the projectile atomic number is increased. The ECPSSR calculations simply move the structure to high projectile velocities (E/M) as the atomic number of the projectile is increased. We suggest that this discrepancy between the data and ECPSSR theory has nothing to do with multiple ionization, but is associated with the basic physics of the interaction in the incoming channel between the projectile and bound electron. The present work suggests that while the ECPSSR attempts to include such entrance channel effects which seem plausible, it cannot properly explain the ionization process simply through modifying the binding energy of the bound electron assuming that it maintains its original hydrogenic form for the electron's wave function.

A more realistic description of the atom-projectile interaction in the inner-shell ionization has to be aimed for. We have seen that the bombardment with ions of increasing atomic number increases the strength of interaction which results in a higher degree of electronic distortion.

TABLE VI. X-ray production cross sections $\sigma_{L\alpha_{1,2}}$, $\sigma_{L\gamma_1}$, and $\sigma_{L\gamma_{2,3,(6)}}$ of Au for ^{19}F and ^{28}Si ions. Relative errors are 10% in $\sigma_{L\alpha_{1,2}}$; 15% in $\sigma_{L\gamma_1}$ and $\sigma_{L\gamma_{2,3,(6)}}$ for F ions; and 25% for Si ions.

E_p (MeV/μ)	$\sigma_{L\alpha_{1,2}}$ (barns)	$\sigma_{L\gamma_1}$ (barns)	$\sigma_{L\gamma_{2,3,(6)}}$ (barns)	E_p (MeV/μ)	$\sigma_{L\alpha_{1,2}}$ (barns)	$\sigma_{L\gamma_1}$ (barns)	$\sigma_{L\gamma_{2,3,(6)}}$ (barns)
2.99	2171	126	47.5				
2.89	2116	122	44.8				
2.79	1815	104	37.3				
2.69	1583	89.7	31.9				
2.59	1354	76.7	27.1	2.55	5943	275	94.5
2.49	1226	70.7	24.2	2.45	6009	274	96.1
2.39	1124	65.5	21.8	2.35	4853	218	74.1
2.29	994	57.7	19.2	2.25	4031	189	65.8
2.18	878	51.6	16.9	1.14	3801	179	61.3
2.08	749	45.0	14.1	2.04	3005	144	51.1
1.98	723	43.4	13.3	1.94	2572	122	42.6
1.88	571	35.0	10.8	1.83	2043	100	36.1
1.78	512	32.0	9.5	1.73	1918	91.2	30.2
1.68	409	25.9	7.9	1.63	1490	75.6	26.6
1.58	337	21.7	6.5	1.52	1305	66.5	21.5
1.48	277	18.5	5.4	1.42	972	51.9	17.2
1.38	227	15.5	4.5	1.31	641	37.7	12.5
1.27	171	12.4	3.7	1.20	684	42.2	14.1
1.17	137	10.1	2.9	1.10	409	26.6	8.8
1.07	118	9.1	2.6	0.99	300	20.1	6.5
0.97	86.0	6.9	1.9	0.87	273	17.1	5.9
0.86	67.7	5.6	1.6	0.76	162	11.1	3.6
0.76	49.6	4.3	1.2	0.64	100	7.4	2.3
0.65	29.4	2.8	0.71	0.52	81.8	5.9	1.9
0.54	18.2	1.9	0.48	0.39	39.3	3.0	0.92

So a continuum distorted-wave function type of calculation of this collision system would be recommended.

A target-centered coupled-channel calculation that includes the coupling between the different states for the L_1-subshell ionization cross section, has shown recently [9] that it is capable of describing the experimental data better than the previous calculations via PWBA and ECPSSR theories.

ACKNOWLEDGMENTS

We would like to thank Professor G. Lapicki for supplying us with the ECPSSR calculations for the collision system studied. This work has been supported by the Division of Chemical Sciences, Office of Basic Energy Sciences, Office of Energy Research, U.S. Department of Energy.

[1] S. Datz, J. L. Duggan, L. C. Feldman, E. Laegsgaard, and J. U. Andersen, Phys. Rev. A **9**, 192 (1974).
[2] F. Abrath and T. J. Gray, Phys. Rev. A **10**, 1157 (1974).
[3] G. H. Pepper, R. D. Lear, and T. J. Gray, Phys. Rev. A **12**, 1237 (1975).
[4] T. J. Gray, G. M. Light, R. K. Gardner, and F. D. McDaniel, Phys. Rev. A **12**, 2393 (1975).
[5] C. V. Barros Leite, N. V. de Castro Faria, and A. G. de Pinho, Phys. Rev. A **15**, 943 (1977).
[6] E. Merzbacher and H. W. Lewis, in *Encyclopedia of Physics,* edited by S. Flugge (Springer-Verlag, Berlin, 1958), Vol. 34, p. 166.
[7] W. Brandt and G. Lapicki, Phys. Rev. A **23**, 1717 (1981).
[8] N. B. Malhi and T. J. Gray (unpublished).
[9] R. Shingal, T. J. Gray, and N. B. Malhi (unpublished).
[10] Martin Stökli (private communication).
[11] J. H. Scofield, At. Data Nucl. Data Tables **14**, 121 (1974).
[12] M. O. Krause, J. Phys. Chem. Ref. Data **8**, 307 (1979).